Evolution of the microstructure, residual stresses, and mechanical properties of W-Si-N coatings after thermal annealing

Cavaleiro, A.; Marques, A.P.; Fernandes, J.V.; Carvalho, N.J.M.; Hosson, J.Th. De

Published in:
Journal of materials research

DOI:
10.1557/JMR.2005.0169

Publication date:
2005

Evolution of the microstructure, residual stresses, and mechanical properties of W–Si–N coatings after thermal annealing

A. Cavaleiro[a] and A.P. Marques
Instituto Ciência e Engenharia de Materiais e Superficies, Dep. de Engenharia Mecânica, Universidade de Coimbra, 3030 Coimbra, Portugal

J.V. Fernandes
Centro de Engenharia Mecânica da Universidade de Coimbra, Dep. de Engenharia Mecânica, Universidade de Coimbra, 3030 Coimbra, Portugal

N.J.M. Carvalho and J.Th. De Hosson
Department of Applied Physics and Netherlands Institute for Metals Research, University of Groningen, Nijenborgh 4, The Netherlands

(Received 19 August 2004; accepted 24 February 2005)

W–Si–N films were deposited by reactive sputtering in a Ar + N_2 atmosphere from a W target encrusted with different number of Si pieces and followed by a thermal annealing at increasing temperatures up to 900 °C. Three iron-based substrates with different thermal expansion coefficients, in the range of 1.5×10^{-6} to 18×10^{-6} K^{-1} were used. The chemical composition, structure, residual stress, hardness (*H*), and Young's modulus (*E*) were evaluated after all the annealing steps. The as-deposited film with low N and Si contents was crystalline whereas the one with higher contents was amorphous. After thermal annealing at 900 °C the amorphous film crystallized as body-centered cubic α–W. The crystalline as-deposited film presented the same phase even after annealing. There were no significant changes in the properties of both films up to 800 °C annealing. However, at 900 °C, a strong decrease and increase in the hardness were observed for the crystalline and amorphous films, respectively. It was possible to find a good correlation between the residual stress and the hardness of the films. In several cases, particularly for the amorphous coating, *H*/*E* higher than 0.1 was reached, which envisages good tribological behavior. The two methods (curvature and x-ray diffraction) used for calculation of the residual stress of the coatings showed fairly good agreement in the results.

I. INTRODUCTION

Tungsten-based coatings deposited by sputtering have many applications such as diffusion barriers,[1] semiconductor devices,[2] and hard coatings.[3] Doping W films with an increasing concentration of elements such as Si and N by sputtering provide the possibility of various structures, i.e., metallic phases, nitrides, and even amorphous structures.[4] In these films, Si is bonded preferentially to N forming an amorphous Si–N phase that, in conjunction with nanograins of W-based phases, gives rise to a nanocomposite material.[5] Two amorphous phases are expected, one rich in Si and the other in W.

Detailed knowledge of the thermal behavior of hard coatings is important because in many applications, the service temperature can reach temperatures up to 1000 °C. Another aspect is the possibility of reaching interesting "nanocomposite" structures by the crystallization of as-deposited amorphous coatings via thermal annealing. Of the several hardening factors intervening for reaching a very high hardness in these films, the residual stresses is one of the most important.[6,7] Taking into account that the residual stress is mainly due to the superposition of intrinsic and thermal components, the study of this characteristic whenever changes in temperatures are present is of great importance. In fact, both components depend on the temperature. Intrinsic stresses originate from the growth of defects or structural mismatch between film and substrate, and thermal stress is related to the difference in the thermal expansion coefficients of the film and the substrate. Both will change during the thermal annealing of the film and consequently lead to changes in its mechanical performance.

In previous work,[8,9] the structural and mechanical behavior of amorphous W–Si–N films with increasing annealing temperatures were studied. After crystallization,

[a]Address all correspondence to this author.
e-mail: albano.cavaleiro@dem.uc.pt
DOI:10.1557/JMR.2005.0169

the films showed an important improvement of the hardness values. Changes in the chemical composition were attributed either to the loss of N from the W–N bond (when formed) or to the interdiffusion between the film and the substrate. Depending on the Si content, the crystallization phases ranged from the body-centered cubic (bcc) α–W, a mixture of this phase with W silicides (W_3Si and W_5Si_3), to only silicides (W_5Si_3 and WSi_2). However, thermal stability studies were not performed on the as-deposited crystalline coatings. Moreover, in spite of the suggestions made concerning the influence of the residual stress on the mechanical properties, measurements were not reported.

The aim of this research was to deposit W–Si–N coatings by sputtering with chemical compositions as similar as possible, but one with a crystalline and another with an amorphous structure after deposition. Three Fe-based substrates with different thermal expansion coefficients were used. The coated samples were annealed at increasing temperatures up to 900 °C, and the chemical composition, structure, residual stresses, hardness, and Young's modulus were studied. A comparative study between two different methods [curvature and x-ray diffraction (XRD)] of measuring residual stresses in hard coatings was also performed.

II. EXPERIMENTAL WORK

A. Deposition technique

The films were deposited from a single W target embedded with 7 or 10 pieces of Si by direct-current (dc) reactive magnetron sputtering with a negative substrate bias voltage of 70 V. The total deposition pressure was 0.3 Pa, and the N_2/Ar partial pressure ratio was 1/4 and 1/3. The coatings, with a thickness of ~3 μm were deposited on 310 (AISI) ($Fe_{52}Cr_{25}Ni_{20}Si_2Mn$), FeCralloy ($Fe_{73}Cr_{22}Al_5$), and INVAR ($Fe_{64}Ni_{36}$) substrates with the following respective characteristics: linear thermal expansion coefficients (20–90 °C): (16–18) × 10^{-6} K^{-1}, 11.1 × 10^{-6} K^{-1}, and (1.7–2.0) × 10^{-6} K^{-1}; hardness $HV_{0.1}$: 2.6, 2.0, and 1.5 GPa; Young's modulus: 200, 220, and 145 GPa. The substrates with dimensions of 70 × 10 × 1 mm were polished with diamond paste down to a particle size of 1 μm, and its surface was ion cleaned with an ion gun before coating deposition. The cleaning procedure included electron heating up to temperatures close to 450 °C and afterwards, Ar^+ bombardment for 8 min (ion gun settings at 20 A and 40 V, substrates at −100 V). During the deposition the substrate temperature was kept close to 450 °C.

Thermal annealing of the coatings was carried out at increasing temperatures up to 900 °C in an Ar + H_2 atmosphere for 1 h at each annealing temperature after the furnace chamber was evacuated down to 10^{-3} Pa.

B. Characterization techniques

The chemical composition of the coatings was determined by Cameca SX-50 Electron Probe Microanalysis (EPMA, Courbevoie, France).

X-ray diffraction (XRD) was performed with Co K_α radiation on a DW 3040 X'pert Philips Diffractometer (Almelo, The Netherlands) to analyze the structure of the films.

The residual stress was determined by two different methods; one based on the curvature or deflection of a coated sample and the other based on the direct measurement of elastic deformations (x-ray diffraction using the $\sin^2 \Psi$ method). In the former, two simple methods were used for the curvature evaluation, optical microscopy and profilometry. With a calibrated optical microscope using a 100× magnification objective lens for the focus procedure, it was possible to measure the deflection of the sample over a total length of 38 mm with an increment of 2 mm. The curvature could then be drawn by taking the distance along the XX′ axis and the height of the focus along the YY′ axis. The profilometer allowed similar curve to be obtained. However, due to limitations on the lateral scanning distance of the equipment, only the central part of the sample was considered over a total length of 17.5 mm. With profilometry, in each sample, two profile scans were taken at two parallel lines separated by 2 mm. In both methods, the sample was placed in a sample holder, always in the same position to assure that exactly the same line was being scanned in the following three measurements done for each sample: bare substrate, after coating deposition, and after thermal annealing. The stress in the coating (σ_f) was calculated from the Stoney's equation as follows[10]:

$$\sigma_f = \frac{E_s}{6(1-\nu_s)} \frac{t_s^2}{t_f} \left(\frac{1}{r_a} - \frac{1}{r_b} \right) \quad , \tag{1}$$

where E_s is Young's modulus of the substrate; ν_s is Poisson's ratio of the substrate; t_s and t_f are thickness of the substrate and film, respectively; and r_a and r_b are the curvature radius of the sample before and after deposition/heat treatment, respectively.

The curvature radius was obtained by polynomial (2nd degree) fitting of the experimental data

$$f(x) = a + bx + cx^2 \quad , \tag{2}$$

being the curvature radius given by[11]

$$r = -\frac{1}{2c} \quad . \tag{3}$$

For the $\sin^2 \Psi$ method, the (211) diffraction line of the bcc α–W phase, the only crystalline phase detected before and after thermal annealing, was used for the measurements.

The hardness and Young's modulus were evaluated by

depth-sensing indentation technique using a Fischer Instruments-Fischerscope (Sindelfingen, Germany) and a MTS Nanoindenter XP (Eden Prairie, MN). In the former, the load P was increased in 60 steps until the indentation load of 50 mN was reached, and the same steps were used during unloading. The hardness and Young's modulus values are a result of at least 10 indentations tests. The final result was corrected in relation to the geometrical defects in the tip of the indenter, thermal drift of the equipment, and uncertainty in the initial contact.[12] The latter instrument has an additional functionality that allows for a continuous stiffness measurement (CSM), wherein the contact stiffness is measured continuously as a function of displacement along with the load. With the CSM method, stiffness data were collected and subsequently used in the calculation of the hardness and modulus. A standard approach—load-unload cycle—was used, where the load was held constant at peak load to allow for compensation of creep, and at 70% of maximum load on unloading for calculation of any thermal drift effects. The measurements were repeated at least twenty times and were all loaded using a loading rate $\dot{P}/P$, of 0.05 s^{-1}.[13]

III. RESULTS AND DISCUSSION

A. Chemical composition

Table I presents the results of the chemical composition of the coatings after deposition, normalized to 100% in relation to W, Si, and N elements. Although not shown, oxygen content lower than 2 at.%, due to contamination, was quantified. Furthermore, vestiges of argon were also detected. As expected, the silicon and nitrogen contents in the as-deposited state increase with the number of Si pieces in the target and the N_2/Ar partial pressure ratio, respectively. No significant differences in the chemical composition were detected for the same film deposited on the three different substrates.

After annealing the coated systems up to 800 °C (Tables II and III), it was observed that the different substrates did not induce any variation on the chemical composition of the films. Moreover, the chemical composition of the films remained almost the same for the different annealing temperatures. Only the amorphous films after annealing at both 700 and 800 °C showed a small loss of N from ~29 to ~22 at.% when compared to the as-deposited state. With reference to previous works on similar films, this loss was surprising.[9,14] For W–Si–N sputtered films, it was demonstrated that N establishes bonds preferentially with Si. Therefore, only after the total amount of Si in the coating is bonded to N, for the case of a stoichiometric ratio of Si_3N_4, will W–N bonds be formed. Thus, by taking into account the chemical composition of as-deposited amorphous films, it would be expected that the entire N was combined with Si (Si/N > 0.75). Previous results showed that only the N bonded to W was lost during thermal annealing due to the very low stability of this bond.[15] Hence, if a small amount of N was lost during thermal annealing at 700 °C, and no further loss occurred at 800 °C, it meant W–N bonds were present in these coatings after deposition.

Annealing at 900 °C causes important changes, particularly concerning the labeled B-film. As demonstrated previously regarding the thermal stability of W–Si–N sputtered films,[9] at high annealing temperatures, interdiffusion between the film and the substrate can occur, leading to the variation of the chemical composition of the former detected during the EPMA analysis. Typically, N can diffuse both outwards and inwards and Fe, Cr, and Ni diffuse outwards to an extent depending on the annealing temperature and the initial chemical composition of the coating.[9,14] Consequently, the changes observed in the N content can be attributed to its outward diffusion from the film to the annealing atmosphere. This result is in accordance to the EPMA measurements. During this process, if nitrogen is accumulated in the surface layers before being liberated to the annealing atmosphere, a very high content can be quantified by EPMA, which only probes less than 1 μm from the surface. If N is already lost for the atmosphere, its content almost vanishes. Moreover, for films annealed at 900 °C, it was not possible to reach the total 100 wt% of elements (the elements that were declared were W, Si, N, and O), which characterizes a valid EPMA analysis. Further, a qualitative survey of the chemical composition of the films with this technique allowed the detection of the elements from the substrate (Fe, Cr, and Ni).

TABLE I. Chemical composition of as-deposited W–Si–N films.

Code	Substrate	Si pieces	P_{N_2}/P_{AR}	Chemical composition (at.%)				Thickness μm	Structure
				W	Si	N	Si/W		
A1	310 (AISI)	10	1/3	49.5	22.2	28.3	0.45	3.2	Amorphous
A2	FeCralloy	10	1/3	50.8	21.0	28.2	0.42	3.2	Amorphous
A3	INVAR	10	1/3	48.6	21.6	29.8	0.44	3.2	Amorphous
B1	310 (AISI)	7	1/4	88.4	5.6	6.0	0.06	2.7	α–W
B2	FeCralloy	7	1/4	87.0	5.4	7.6	0.06	2.7	α–W
B3	INVAR	7	1/4	89.1	5.8	5.2	0.06	2.7	α–W

TABLE II. Evolution of the chemical composition and structure of the amorphous W–Si–N film after thermal annealing.

T (°C)	Substrate	Film	Chemical composition (at.%)				Structure
			W	Si	N	Si/W	
700	310 (AISI)	$W_{55}Si_{22}N_{23}$	54.8	22.1	23.1	0.40	Amorphous
	FeCralloy	$W_{55}Si_{23}N_{22}$	55.4	22.5	22.1	0.41	Amorphous
	INVAR	*	…	…	…	…	Amorphous
800	310 (AISI)	$W_{56}Si_{22}N_{22}$	56.3	22.3	21.4	0.39	Amorphous
	FeCralloy	$W_{55}Si_{22}N_{23}$	54.6	22.4	23.0	0.41	Amorphous
	INVAR	$W_{58}Si_{21}N_{21}$	58.3	21.1	20.6	0.36	Amorphous
900	310 (AISI)	$W_{65}Si_{21}N_{14}$	64.8	20.9	14.3	0.32	α–W
	FeCralloy	$W_{60}Si_{21}N_{19}$	59.7	21.6	18.7	0.36	α–W
	INVAR	$W_{58}Si_{21}N_{21}$	58.3	21.1	20.7	0.36	α–W

* Not determined.

TABLE III. Evolution of the chemical composition and structure of the crystalline W–Si–N film after annealing at increasing temperatures.

T (°C)	Substrate	Film	Chemical composition (at. %)				Structure
			W	Si	N	Si/W	
700	310 (AISI)	$W_{88}Si_5N_7$	87.8	5.2	7.0	0.06	α–W
	FeCralloy	$W_{88}Si_6N_6$	88.2	5.6	6.2	0.06	α–W
	INVAR	*	…	…	…	…	α–W
800	310 (AISI)	$W_{88}Si_6N_6$	88.4	6.2	5.4	0.07	α–W
	FeCralloy	$W_{89}Si_6N_5$	88.7	6.4	4.9	0.07	α–W
	INVAR	$W_{88}Si_7N_5$	88.8	6.6	4.6	0.06	α–W
900	310 (AISI)	$W_{91}Si_7N_2$	91.4	6.6	2.0	0.07	α–W
	FeCralloy	$W_{94}Si_6N_{0.16}$	94.1	5.7	0.2	0.06	α–W
	INVAR	$W_{55}Si_4N_{41}$	55.1	4.3	40.6	0.08	α–W

* Not determined.

B. Structure

The structure of the films depends on the concentration of Si and N. The as-deposited film with higher Si and N content (A-film from Table I) has an amorphous structure, whereas the B-film exhibits the bcc α–W phase (e.g., Fig. 1 for 310 steel substrate). The formation of amorphous materials of metal–metalloid type,[16] such as W–Si–N coatings, depends on the difference in the atomic size, the strength of the bonding between the metal and the metalloid, and the probability of forming intermetallic compounds with different structures. In the W–Si–N system, the heterogeneity of the atomic size between the three elements is high, and with increasing concentration of silicon and nitrogen, the formation of Si–N bonds is enhanced. Therefore, the probability of the formation of an amorphous structure is enhanced with increasing silicon and nitrogen. Other authors have reached similar results for this system[17] and for the Mo–Si–N system.[18]

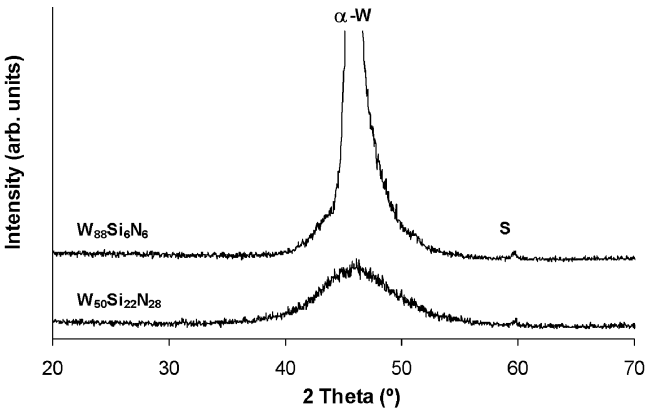

FIG. 1. XRD patterns of the W–Si–N films deposited on the 310 (AISI) steel substrate after deposition.

After thermal annealing at temperatures up to 800 °C, no significant changes in the XRD patterns were observed. Only small shifts in the peak position and a narrowing of the diffraction peaks could be detected. At 900 °C, the A-film crystallized as α–W phase. No other crystalline peaks were detected for all the substrates and annealing temperatures. The result suggests that Si-containing phases are amorphous and remain in this metastable state even after annealing at the highest temperatures studied. The crystallization of Si–N amorphous phases is known to occur only for temperatures above 1000 °C.[19] The absence of W–N phases after annealing can be justified, as mentioned previously, by the preferential bonding between Si and N. Even considering that after deposition the entire N content is not exclusively bonded to Si, the very low stability of the W–N bond with the temperature prompts the release of N during the

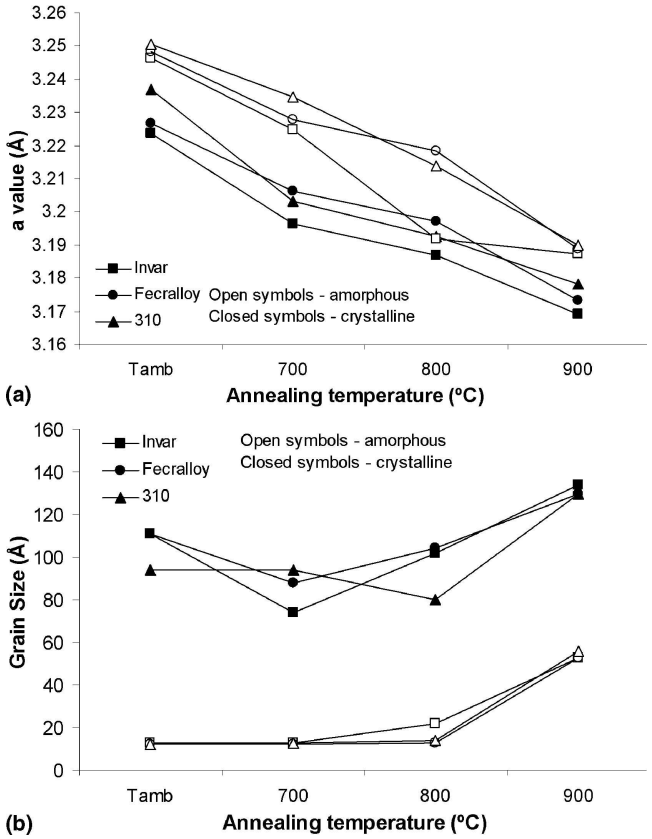

FIG. 2. (a) Lattice parameter and (b) grain size of both A and B W–Si–N films before and after annealing at increasing temperatures.

thermal annealing, resulting in bcc α–W as the only crystalline phase detected.

Figure 2 shows the evolution of the lattice parameter and grain size of both films, deposited on the three substrates as a function of the annealing temperatures. The XRD pattern of the amorphous films were treated as being from a crystalline material, assuming the main broad diffraction peak could be assigned to the (110) plans of a bcc phase. Scherrer's formula, taking the integral width of the diffraction peaks, was used for grain size calculation.[20] The main observations obtained taken from the analysis of Fig. 2 are as follows.

In all cases, including the amorphous films, there is a continuous decrease of the lattice parameter, which is always higher than the International Center for Diffraction Data (ICDD) standard value for α–W phase with the increasing annealing temperature. This continuous trend was also observed when crystallization occurred in the amorphous film. This fact points out that clusters of atoms with an atomic arrangement close to that found in the bcc α–W phase should already exist in amorphous films. The dilatation of the lattice parameter in relation to the ICDD standard value can be attributed to two factors: the residual stresses (the higher the compressive stress, the higher the lattice parameter) and the presence of atoms of different elements in metastable positions in the W-lattice. As mentioned above, impurity atoms such as oxygen and carbon, coming from contaminants during the deposition process, atoms of the processing gas (argon), and Si and N atoms, which did not have enough time to segregate and bond preferentially each other, remain in the W-lattice after deposition. As will be shown later on, in some cases the stresses do not decrease with increasing annealing temperature. Thus, the decrease in the lattice parameter observed in Fig. 2(a) should be attributed to the out diffusion of the atoms placed in metastable positions in the W-lattice to the grain boundaries, for example.

For all annealing temperatures, the films deposited on the INVAR substrates showed a smaller lattice parameter than those deposited on the other alloys due to their lower compressive residual stress values, as will be shown later on.

After crystallization, the lattice parameter of the bcc α–W phase is higher than that of the crystalline film annealed at the same temperature.

There is no significant change in grain size for both films after annealing at temperatures up to 800 °C. Besides the obvious increase in the grain size after crystallization of the amorphous film, at 900 °C a small increase in this structural parameter was also registered for the crystalline film at this temperature.

The grain size in the crystallized A-film is much smaller than in as-deposited B-films.

C. Residual stress

1. Analysis of reliability of stress results

The use of different methods for the stress evaluation of coatings allows the identification of inadequacies. In relation to the stresses calculated from the deflection of a coated bar, Fig. 3 shows the values determined by applying directly the Stoney's equation to the curvature

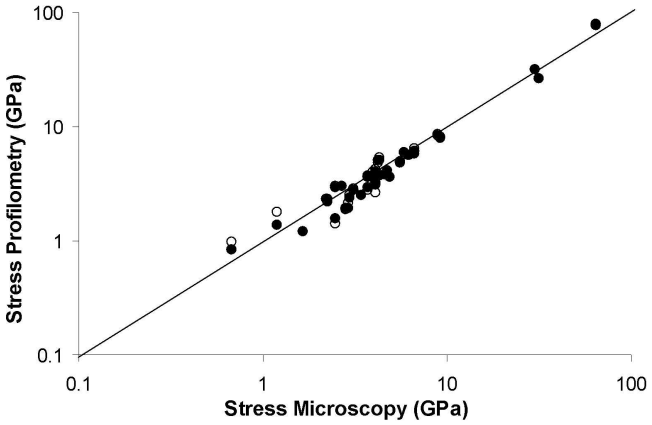

FIG. 3. Comparison between the stress values calculated from the deflection of a coated sample measured by optical microscopy and by profilometry methods (open and close symbols corresponds to profilometry measurements taken in two different parallel lines along the length of the sample).

radii of both films deposited into the three different substrates before and after annealing at increasing temperatures. The curvature was measured by profilometry, along two lines parallel to the length of the sample (open and closed symbols) and by optical microscopy. There are almost no differences between the position in the plot of open and closed symbols, meaning that the position for the scan measurement on the width of the sample does not seem to be very important for the curvature measurements.

Good correlation was also found between the stresses calculated from the curvatures measured by both profilometry and optical microscopy techniques. The small differences can be attributed to local distortions of the substrate surface uniformity during sample preparation. In the profilometry technique, the scans are shorter than for the microscopy method (17.5 mm versus 38 mm). Thus, the profilometry scans are more sensitive to these distortions with the consequent differences in the stress calculation. The highest discrepancies were reached for the INVAR substrate.

The application of the deflection method without a critical sense of the results can be misleading. Figure 3 shows some stress values that are rather impossible, such as 30 and 60 GPa. Some of the inappropriate values were calculated from the curvatures of the FeCralloy substrate coated with the as-deposited crystalline B-film after thermal annealing at 700 and 800 °C. These samples displayed very small curvature radii, which can be explained only if plastic deformation of the substrates took place during the annealing process.

At this point, the main question is why the FeCralloy samples plastically deform more extensively than the 310 (AISI) or INVAR alloys, regardless of its higher yield strength. The residual stresses in these films are a consequence of two contributions: the intrinsic stresses due to the growing process of the film and the thermal stresses due to the mismatch in the thermal expansion coefficients between the film and the substrate. During thermal annealing, even if thermal stresses are annihilated, the intrinsic stresses of the films exert their influence on the substrates. However, as can be observed in Fig. 4 (data from Ref. 21), the mechanical strength of the alloy Fe–27% Cr, with chemical composition close to FeCralloy, decreases with an increase of temperature more steeply than the other two substrates. For example, at 600 °C its yield strength is already lower than the value of the other alloys. Moreover, as it will be presented later, the B-film deposited onto FeCralloy has a higher compressive stress than when it is deposited onto the other substrates, which has been attributed to a high level of intrinsic stress component.

It is not easy to estimate the stresses that can be present at the film when the coated sample is annealed at increasing temperatures. Only if the film stress value is known will it be possible to calculate the maximum stress developed in the substrate by using, for example, the analysis of Townsend et al.[22] By combining Eqs. (32a) and (32b) deduced in their paper and considering $z = t_s$, the maximum stress in the substrate can be calculated from

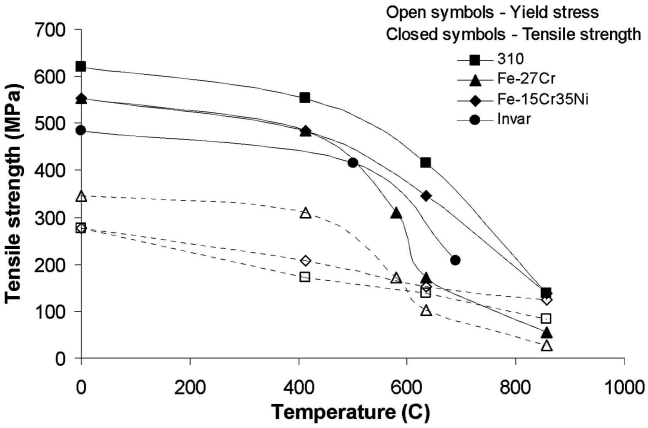

FIG. 4. Evolution of the mechanical strength of different Fe-based alloys at increasing temperatures.[21]

$$\sigma_s = -4\sigma_f \frac{t_f}{t_s} \quad , \tag{4}$$

where σ_s and σ_f are the stress in the substrate and in the film, respectively; and t_s and t_f are the thickness of the substrate and film, respectively.

The stress in the film at a given annealing temperature can be estimated by considering the stress value measured after cooling down from this temperature and subtracting the thermal stress component. The last one can be calculated from[22]

$$\sigma_{Therm} = \frac{E_f}{(1-\nu_f)}(\alpha_f - \alpha_s)\Delta T \quad , \tag{5}$$

where E_f is Young's modulus of the film; ν_f is Poisson's ratio of the film; σ_{Therm} is the thermal stress component; α_s and α_f are thermal expansion coefficients of the substrate and film, respectively; and ΔT is the temperature range.

Thus, by considering for B film deposited on FeCralloy substrate and annealed at 700 °C, $E_f = 430$ GPa, $\nu_f = 0.25$, $\alpha_s = 14 \times 10^{-6}$ K^{-1}, $\alpha_f = 7 \times 10^{-6}$ K^{-1}, we arrive at $\sigma_{Therm} = 2.8$ GPa. Taking into account that for this film the experimental value of the stress measured at room temperature was −7.2 GPa, the stress at 700 °C should be $\sigma_f = -7.2 + 2.8 = -4.4$ GPa. Then, for $t_s = 0.82$ mm and $t_f = 2.8$ μm, the value of σ_s is at about 60 MPa. This value is very close to the yield strength of an alloy with chemical composition similar to FeCralloy at 700 °C (see Fig. 4). Thus, during the annealing at high temperatures, the residual stresses in the coatings can be high enough to induce plastic deformation of the substrate impeding the application of Stoney's method for

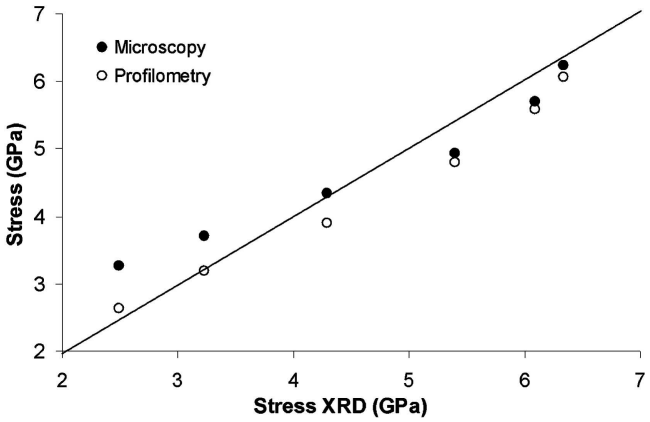

FIG. 5. Comparison between the stress values measured in the crystalline W–Si–N film deposited on FeCralloy, 310 (AISI) steel, and INVAR substrates, calculated from the deflection of a coated sample and from XRD $\sin^2\psi$ methods.

the calculation of the film stress which, obviously, is valid only in the elastic regime.

To overcome the problems related to the plastic deformation of the substrates, the stresses in crystalline films were evaluated by XRD. The Young's modulus of the films necessary for the stress calculation was determined by depth-sensing indentation. For the cases where a comparison could be made (those for which plastic deformation of the substrate was not likely), Fig. 5 shows the comparison between the stress values calculated from the deflection and XRD methods. Taking into account the uncertainties on the E values by depth-sensing indentation, a good agreement in the values determined by both methods is found.

Figure 6 shows a macrograph of the FeCralloy samples coated with the crystalline B-film, annealed at different temperatures. The (radius of) curvature of the specimens is defined as positive when the coated surface is convex. For positive curvature, the residual stress in the film whenever the Stoney's method is applicable, is compressive. With the increase of the temperature, the curvature became more pronounced, and suddenly at 900 °C the signal was inverted. As can be observed at 800 °C, the curvature of the coated sample is really very pronounced confirming the suggested plastic deformation of the substrate as referred to above. Up to 800 °C,

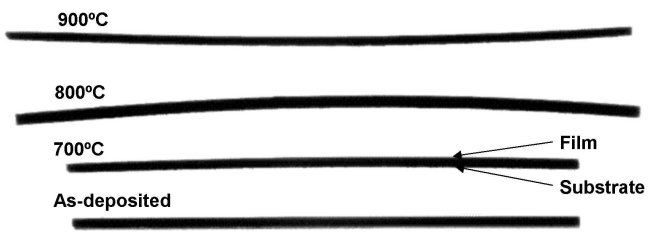

FIG. 6. Macrograph of the curvatures of the crystalline W–Si–N coating deposited on the FeCralloy substrate and annealed at increasing temperatures.

the curvature is positive, and then at 900 °C, the curvature becomes negative which should represent tensile stress. An interesting point to be noted is the fact that regardless of the negative curvature of these coated samples (a similar situation is also observed for B-film coated INVAR substrate), their XRD analysis allows calculation of compressive stress values. This incongruence can only be explained if somewhere between 800 and 900 °C the action of the different factors intervening in the residual stress of the coatings (difference in the thermal expansion coefficients, annihilation of intrinsic residual stress by the effect of temperature, changes in the chemical composition due to the interdiffusion between the film and the substrate, etc.) induces a change in the signal of the residual stresses, from negative (compressive) to positive (tensile). The very low strength of the substrate material at that temperature makes its plastic deformation very easy, and the residual tensile stress in the coating leads to the deflection of the coated sample. The estimation of these stresses is even more difficult than for the case presented above (B-film coated FeCralloy substrate at 700 °C) since more and more parameters are being intervening in the process as the temperature is increasing. However, the inversion in the curvature of the coated sample after heating at 900 °C can be explained only by the occurrence of tensile stresses in the film. During cooling down to room temperature, the difference in the thermal expansion coefficients between the film and the substrate will again exert its influence, creating, in these cases, compressive stresses. However, as the substrate mechanical strength rapidly increases with decreasing temperature, the created compressive stresses in the coating are not sufficiently high to promote plastic deformation of the substrate, and the induced elastic deformation is not high enough to annihilate the negative curvature acquired by the coated samples at 900 °C annealing. In conclusion, if plastic deformation may occur during the annealing process, at room temperature the coated sample can show a curvature typical of tensile stress but staying under compressive stress.

A detailed observation of the films surface permitted the detection of extensive cracking in the film. Concerning the coated system with FeCralloy substrate, only longitudinal cracks could be observed, whereas a network of cracking characterized the films deposited on the other substrates. In the film deposited on INVAR substrate, only some transversal cracking connecting the longitudinal cracks are detected. However, as shown in Fig. 7, where the aspect of the cracked film deposited on 310 steel and FeCralloy substrates is compared, the density of transversal and longitudinal cracks is very similar for the 310 steel substrate. In the case of the film deposited on INVAR, the calculation of the stresses by XRD along three directions: 0°, 45°, and 90° with respect to the longitudinal cracks, led to values of 2.23, 1.98, and

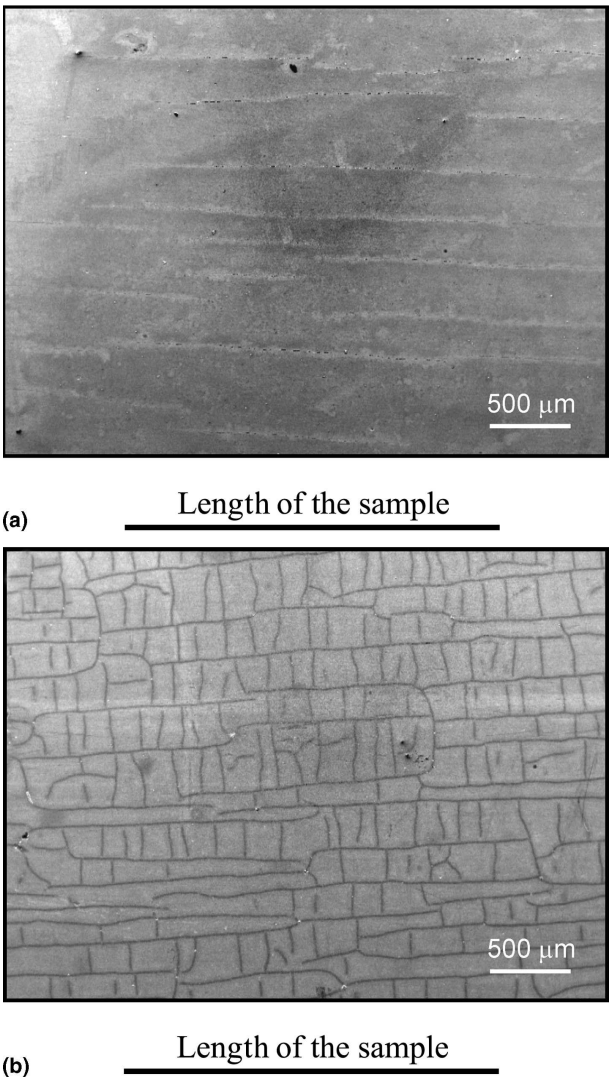

FIG. 7. Cracking detected on the crystalline W–Si–N coating after it has been annealed at 900 °C when deposited (a) on FeCralloy substrate and (b) on 310 (AISI) steel.

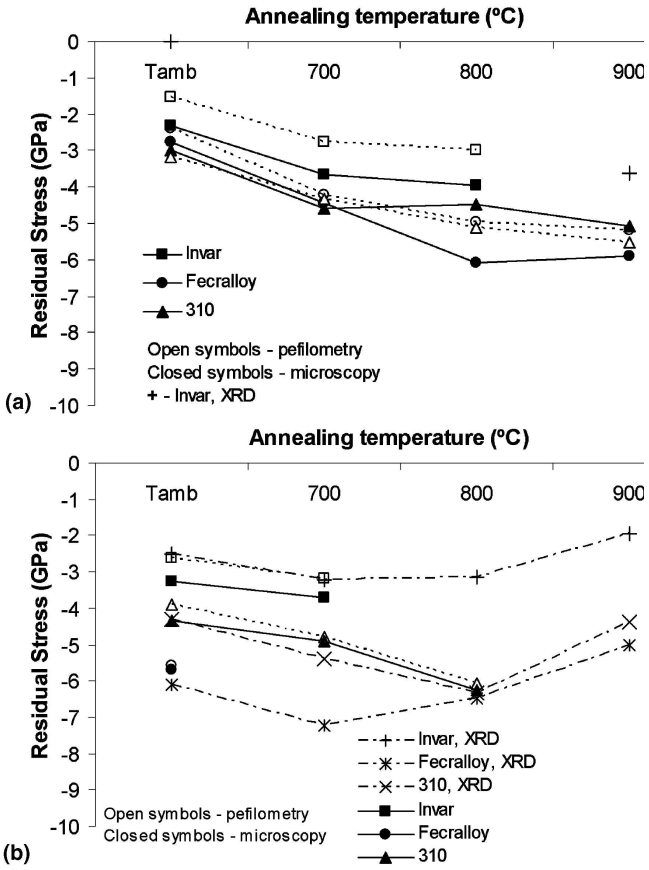

FIG. 8. Residual stress of both A and B W–Si–N films deposited on FeCralloy, 310 (AISI) steel, and INVAR substrates before and after annealing at increasing temperatures: (a) as-deposited amorphous film and (b) as-deposited crystalline film.

1.95 GPa, respectively. Therefore, only a small decrease is observed from 0° to 90°, which is probably due to stress relaxation induced by the cracking in the film. The observed cracking in B film at 900 °C is one more reason that confirms unequivocally the presence of tensile stresses occurring in the film at this temperature. The reason longitudinal cracking is preferential in relation to transversal cracking should be due to the stress distribution in the film related to the shape of the sample. This subject is currently under investigation.

In the amorphous W–Si–N film, none of these events were observed. Even when the samples were annealed at 900 °C, no cracks of any type were detected. Two main factors can justify this different behavior. First, amorphous film is tougher and more ductile than crystalline film; in a previous study it was shown that amorphous W-based sputtered coating has a lower tendency for cracking than crystalline films when they were submitted to scratch-testing, which may indicate a higher toughness of the amorphous coatings.[23] Second, the difference in the thermal expansion coefficients between the film and the substrate is not so high for the case of amorphous film, which shows that, during the heating, the induced thermal stress is not high enough to annihilate the compressive stress existing in the film after deposition.

2. Stress values

Figures 8(a) and 8(b) plot the measured stress values using different methods for the amorphous and the crystalline films, deposited on the three substrates, as a function of the annealing temperatures. In all cases, compressive stresses were determined. For the values resulting from the use of Stoney's method, only those considered valid (when plastic deformation of the substrate did not occur) are presented. The compressive stress induced in the coatings arises from both the intrinsic contribution associated to the ion bombardment and growing of the coatings during the deposition process, and from the thermal contribution due to the difference between the

thermal expansion coefficients of the film (α_f) and of the substrate (α_s) during the cooling from the deposition temperature (~450 °C). The ion bombardment promotes the incorporation of the discharge gas (argon) into the film lattice enhancing the denominated "atomic peening effect,"[24] in which the energetic atoms promote the densification of the film and thus an increase of the compressive stress. Moreover, whenever either growth of films with epitaxial relationships or attractive forces between the columns in low density films occur, stresses can be developed in the coatings.[25] The deposition of very compact films with low discharge pressure and negative substrate bias improves the ion bombardment and consequently induces compressive stress in the films. The difference between α_f and α_s can also induce compressive stresses in the coating after cooling since α_s, which is as high as 18×10^{-6} K^{-1}, is much higher than α_f [$(3–7) \times 10^{-6}$ K^{-1}].[26] The latter value was taken by considering the thermal expansion coefficients of bulk materials formed by compounds of the elements constituting the film (tungsten silicide, tungsten nitride and silicon nitride). It is also important to mention that in many films, the α_f values calculated are lower than those of the corresponding bulk material, as is the case of silicon nitride thin films.[27] Furthermore, the usually presented low α value for INVAR alloys concerns low temperature ranges. For example, the linear coefficient of thermal expansion is 1.2, 4.9, and 13.9×10^{-6} K^{-1} in the ranges 30–100, 30–300, and 30–900 °C, respectively.[28] Thus, as the range of annealing temperatures studies reaches 900 °C, an important difference could also be expected in the thermal expansion coefficients between the films and the INVAR substrates.

Considering the different α_s values, the first important conclusion of the analysis of both figures is that in all cases the films deposited on INVAR substrates showed a lower stress values than the correspondent films deposited on the other alloys. This result is in agreement with the lower lattice parameter measured for those films (see Fig. 2). In fact, the in-plane compressive stress leads to a decrease of the interplanar distance for the lattice plans perpendicular to the substrate. Using elasticity theory, this corresponds to an increase of the interplanar distance of the lattice planes parallel to the substrate. As these are the only possible planes detected by conventional XRD diffraction technique, a decrease of the compressive stresses should induce a decrease of the interplanar distances calculated from the XRD analysis. As the films were deposited at temperatures close to 450 °C, during the cooling down to room temperature the thermal component of the stresses in the films should be more compressive in the cases of 310 (AISI) steel substrates and FeCralloy than with INVAR.

For example, if the difference of α_s values between INVAR and the 310 steel substrate is taken to be close to 10×10^{-6} K^{-1} and the Young's modulus of the film to be 350 GPa (see Sec. III. D), a temperature difference of 450 °C gives rise to a thermal stress value of ~1 GPa if Eq. (5) is used. This value is on the same order of magnitude as the differences in the stress observed in Fig. 8 for films deposited on 310 (AISI) steel and INVAR substrates. Considering only the amorphous films [see Fig. 10(a)], a similar trend is observed between 310 (AISI) steel and FeCralloy substrates. Indeed, a higher compressive stress is measured in the film deposited on the 310 steel, which is due to its higher α_s value than the one of FeCralloy. On the other hand, the crystalline B-film deposited on the latter substrate [see Fig. 8(b)] has not only a very large difference in the stress value in relation to the one deposited on the INVAR alloy but also a value even higher than that when it is deposited on 310 (AISI) steel. This fact should be attributed to the magnitude of the intrinsic component of the stress. The film has a structure similar to that of the FeCralloy substrate. Both have a simple bcc metallic lattice in contrast to the other substrates, which are characterized by the face-centered cubic (fcc) austenite γ-phase. During film growth, epitaxial relationships could then be expected for FeCralloy substrates. The larger atomic radius of W in relation to Fe induces a lattice distortion in the films if epitaxial growth occurs. Compressive stresses are then created to compensate for the mismatch between the atomic radii of the film and FeCralloy substrate. This is not expected when the crystalline film is deposited onto the other substrates.

With increasing annealing temperatures up to 800 °C, the compressive stress develops smoothly. This behavior is unusual whenever high compressive stressed films are annealed. In literature, a decrease of the residual stresses is usually reported (see for example, Ref. 29), as being attributed mainly to either structural relaxations or losses of loosely bonded atoms or molecules of the discharge gas or contaminant elements. Furthermore, this would be the expected behavior since, as shown in Fig. 9 where the stress free lattice parameters of the crystalline films calculated from the XRD $\sin^2\psi$ method are presented, the plotted values decrease from the room temperature to 700 °C and then are kept constant for higher annealing temperatures. This value is very close to the standard ICDD value of α–W (3.1648 Å[30]) and is independent of the substrate on which the film is deposited. The trend reflects initially the liberation or segregation of the loosely bonded atoms and later, the absence of other chemical species in the W-lattice.

The increase in the compressive residual stresses is considered to be related to an increasing contribution of the thermal component to the total stress value. During the stage at the annealing temperature, any thermal stresses will be relaxed, and during the cooling down to room temperature, new compressive stresses are created due to the difference in the thermal expansion coefficients

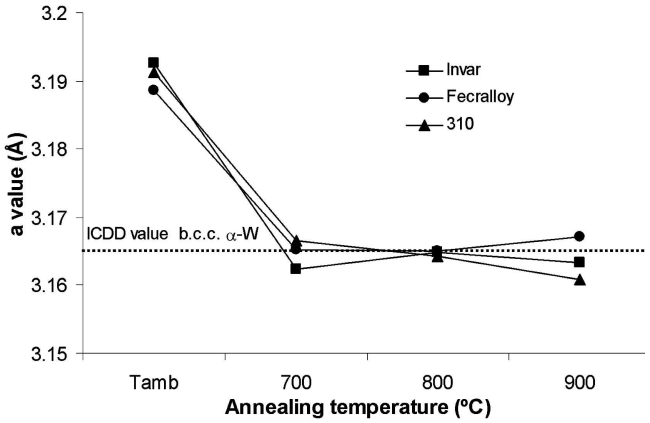

FIG. 9. Stress-free value of the lattice parameter of the crystalline W–Si–N film deposited on FeCralloy, 310 (AISI) steel, and INVAR substrates after annealing at increasing temperatures.

of the film and the substrate, whose magnitude will depend on the annealing temperature.

D. Mechanical properties

Figures 10(a) and 10(b) show the evolution of the hardness (H) and Young's (E) modulus values of the films as-deposited and after annealing. These data were obtained using a Fischer Instruments ($L_{max} = 50$ mN). In these conditions, the ratio of maximum penetration depth to film thickness is, in all cases, smaller than 0.11, assuring that no influence of the substrate occurred during the hardness evaluation of the film.[31] However, to access the validity of such values, a series of samples were also tested using a MTS Nanoindenter® XP equipped with the CSM module using either a Vickers or a Berkovich tip. In this last case, the results were taken from the region of the hardness curve versus penetration depth, corresponding to low applied loads where constant hardness values are calculated and no influence of the substrate is detected. No significant variations in H and E values using both equipments and indenter tips were registered, the differences being only in the statistical errors inherent to each technique. Furthermore, no systematic tendency is registered in the values measured by each apparatus; i.e., in some cases the values were higher for one type of equipment, and in other cases, the inverse occurred.

The annealing temperature up to 800 °C had no significant influence on the H and E values; only small changes were detected. On the other hand, at 900 °C, there is a steep variation for both films deposited on the three substrates. Inverse trends for the amorphous and the crystalline films were observed. In the former, there is a strong increase, which is believed to be associated with the crystallization process. The values obtained after crystallization are very close to those of the as-deposited crystalline films, about 40 GPa, which is a remarkable value for a film constituted preferentially by a single metallic bcc phase. As shown previously in Fig. 9, the stress free value of the lattice parameter is very close to the ICDD standard of the α–W phase, which confirms its purity. The conjunction of high compressive stresses with the very low grain size of the structure associated with hard and amorphous Si-rich phases is a factor that should be taken in account for the justification of the high hardness values found. Further, for the latter, the influence of the interdiffusion between the film and the substrate supports the interpretation of the sudden decrease of the hardness when annealed at 900 °C.

It is well known that residual stresses can have a predominant role in the hardness of thin sputtered films.[32] In many studies, close correlation between the stress and the hardness has been found. Although many other factors can influence the hardness values, Fig. 11 demonstrates that, globally, the coatings with higher compressive residual stresses are harder. For each coated system, the stress values calculated with the different used methods are presented. Two groups of data can be considered, depending on the structure of the films. The influence of

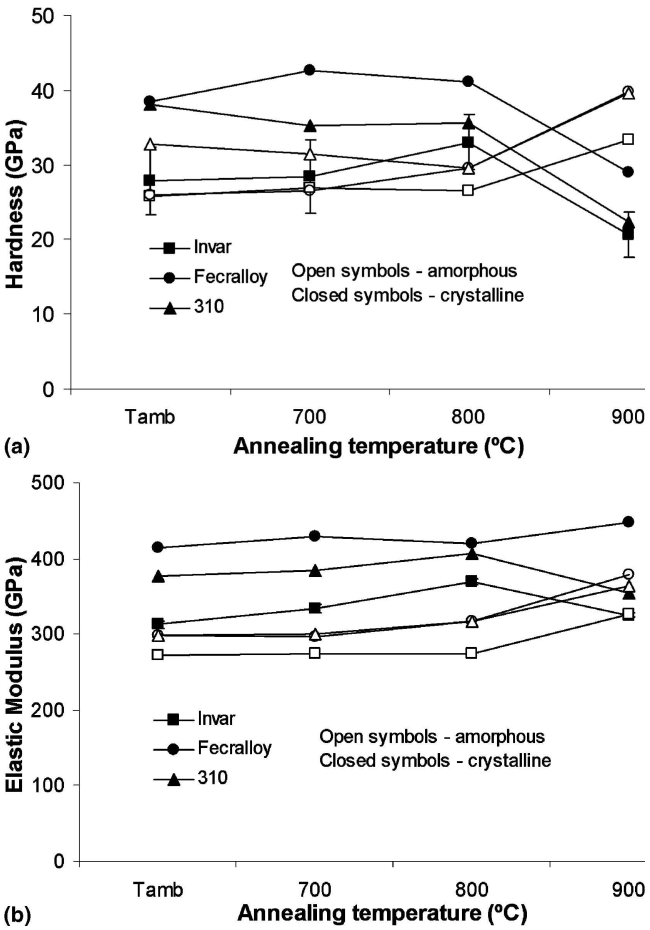

FIG. 10. (a) Hardness and (b) Young's modulus of both A and B W–Si–N films deposited on FeCralloy, 310 (AISI) steel, and INVAR substrates and annealed at increasing temperatures (error bars are shown as an example for one case).

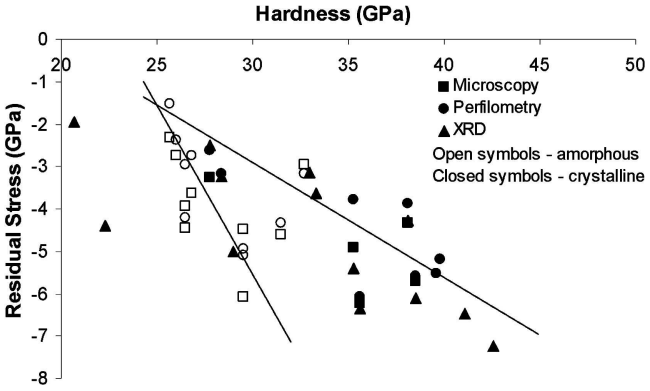

FIG. 11. Hardness values of both A and B W–Si–N films deposited on FeCralloy, 310 (AISI) steel, and INVAR substrates and annealed at different temperatures as a function of the residual stresses.

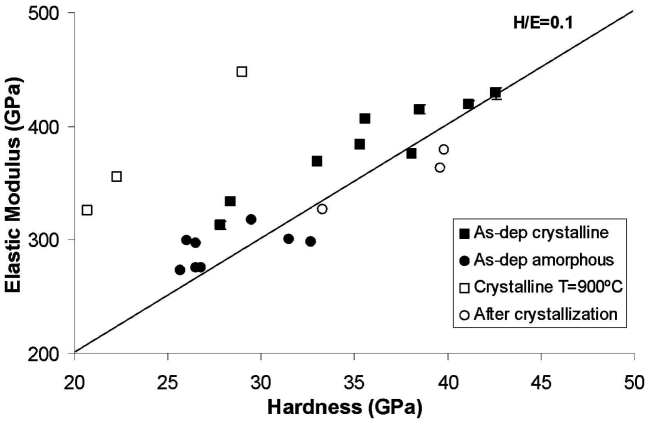

FIG. 12. Young's modulus of both A and B W–Si–N films deposited on FeCralloy, 310 (AISI) steel, and INVAR substrates and annealed at different temperatures plotted as a function of the hardness values.

the residual stresses seems to be more effective in the crystalline than in amorphous films. A strong increase in the compressive stress values (from 2 to 6 GPa) leads to a hardness increase of the former by 20 GPa, whereas in the latter, the increase is no more than 7–8 GPa. These different trends should be related to the characteristic deformation mechanisms typical of both amorphous localized shear bands) and crystalline (dislocation gliding and/or grain boundary sliding) materials.

Similarly, many researchers have been trying to relate empirically the hardness with the grain size. Even if the well-known Hall–Petch relationship does not hold for this type of films given the exceptional low values of the grain size (nanometer range), many authors[33,34] found that it can be applicable for films with decreased grain size. To this end, it would be necessary that grain boundary sliding were hampered. The chemical composition result shows that the interdiffusion between the film and the substrate is expected at 900 °C. Although not detected in this study by XRD, previously[9,14] formation of "new" phases consisting of elements from the film and the substrate, such as Fe_2W and NiWSi, was observed. Moreover, the element distribution across the thickness of the films showed that in particular zones, the N content completely vanished. Both of these results allow the assumption that the interdiffusion can lead to the destruction of the above-mentioned nanocomposite structure. Therefore, in addition to the effects of the residual stresses and grain size variations, a structural transformation related to the interdiffusion can also contribute to the decrease of the hardness observed for annealing at 900 °C.

The relationship between the hardness and the Young's modulus for all films is shown in Fig. 12. The approximate linear trend between the values of these two properties is typical for this type of hard coatings and reveals a brittle behavior (see, for example, Ref. 35). The data points shifted from the trend correspond to the crystalline film deposited on the three substrates after it is annealed at 900 °C. The dissimilarity between the behavior of these composite systems and the other samples confirms the alteration of the chemical composition due to the interdiffusion phenomenon.

The analysis of Fig. 12 allows the conclusion that the higher *H*/*E* ratios are reached in coatings that originally have as-deposited amorphous structure. Even after crystallization, these coatings present *H*/*E* ratios higher than the crystalline as-deposited coatings. In these cases the *H*/*E* ratio is higher than 0.1, which shows a potentially promising tribological behavior as noted by several authors.[36,37] Therefore, the production of nanocomposite coatings by crystallization induced during thermal annealing can be an excellent alternative with respect to their direct deposition.

IV. CONCLUSIONS

This paper represents a study of the thermal stability of two W–Si–N coatings with similar chemical compositions, one with amorphous and another with crystalline structures. The following conclusions can be drawn.

Independent of the Si concentration, the only crystalline phase detected for the films, including the one resulting from the crystallization of the amorphous film at 900 °C, was the bcc α–W phase, suggesting that an amorphous Si-nitride should exist, forming a nanocomposite material.

Good agreement was found between the residual stress values calculated using Stoney's equation applied to the deflected coated samples and the XRD $\sin^2 \Psi$ method. It was also demonstrated that the application of deflection method could be problematic if plastic deformation of the substrate occurs, as is most probable in thermal annealing studies.

In all cases, compressive stresses were measured in the coatings. The films deposited on INVAR presented systematically lower values than those on the other

substrates due to its lower thermal expansion coefficient. In the case of crystalline film deposited on FeCralloy, such a trend was not observed due to intrinsic stress induced by epitaxial growth.

Contrary to what could be expected, with thermal annealing, there was a smooth increase of the compressive stress values; for crystalline film only, for the highest annealing temperatures, a small decrease in the stress was detected.

For annealing up to 800 °C, there were no significant changes in the hardness and Young's modulus of the coatings. However, at 900 °C, the hardness increased steeply for the amorphous film, probably due to the crystallization, whereas it decreased for the crystalline film. In many cases a value of H/E higher than 0.1 was found, suggesting good tribological behavior.

Good correlation between the hardness and the residual stress was found.

ACKNOWLEDGMENTS

This research was sponsored by the Portuguese Foundation for Science and Technology (Fundação para a Ciência e Tecnologia, Portugal) through Fundo Europe de Desenvolvimento Regional (FEDER) as part of program Programa Operacional "Ciência, Technologia e Inovacão" (POCTI) 33978/99.

REFERENCES

1. J.G. Fleming, E. Roherty-Osmun, P.M. Smith, J.S. Custer, Y-D. Kim, T. Kacsich, M-A. Nicolet, and C.J. Galewski: Growth and properties of W–Si–N diffusion barriers deposited by chemical vapor deposition. *Thin Solid Films* **320,** 10 (1998).
2. J.S. Reid, E. Kolawa, R.P. Ruiz, and M-A. Nicolet: Evaluation of amorphous (Mo,Ta,W)–Si–N diffusion barriers for ⟨Si⟩/Cu metallizations. *Thin Solid Films* **236,** 319 (1993).
3. L.R. Shaginyan, M. Misina, J. Zemek, J. Musil, F. Regent, and V.F. Britun: Composition, structure, microhardness and residual stress of W–Ti–N films deposited by reactive magnetron sputtering. *Thin Solid Films* **408,** 136 (2002).
4. C. Louro and A. Cavaleiro: Hardness versus structure in W–Si–N sputtered coatings. *Surf. Coat. Technol.* **116/119,** 74 (1999).
5. C. Louro, A. Cavaleiro, and F. Montemor: How is the chemical bonding of W–Si–N sputtered coatings? *Surf. Coat. Technol.* **142–144,** 964 (2001).
6. T.Y. Tsui, W.C. Oliver, and G.M. Pharr: Influence of stress on the measurement of mechanical properties using nanoindentation: Part I. Experimental studies in an aluminium alloy. *J. Mater. Res.* **11,** 752 (1996).
7. A. Bolshakov, W.C. Oliver, and G.M. Pharr: Influence of stress on the measurement of mechanical properties using nanoindentation: Part II. Finite element simulations. *J. Mater. Res.* **11,** 760 (1996).
8. C. Louro and A. Cavaleiro: Mechanical behaviour of amorphous W–Si–N sputtered films after thermal annealing at increasing temperatures. *Surf. Coat. Technol.* **123,** 192 (2000).
9. A. Cavaleiro and P. Marques: Structural and mechanical properties of amorphous W–Si–N sputtered films after thermal annealing. *Thin Solid Films* **441,** 150 (2003).
10. G.G. Stoney: The tension of thin metallic films deposited by electrolysis. *Proc. R. Soc. London Ser. A* **82,** 172 (1909).
11. P.M. Ramsey, H.W. Chandler, and T.F. Page: The determination of residual stresses in thin coatings by a sample thinning method. *Surf. Coat. Technol.* **43–44,** 223 (1990).
12. J.M. Antunes, A. Cavaleiro, L.F. Menezes, M.I. Simões, and J.V. Fernandes: Hardness ultra-microhardness testing procedure with a Vickers indenter. *Surf. Coat. Technol.* **149,** 27 (2002).
13. N.J.M. Carvalho and J.Th.M. De Hosson: Characterization of mechanical properties of tungsten carbide/carbon multilayers: Cross-sectional electron microscopy and nanoindentation observations. *J. Mater. Res.* **16,** 2213 (2001).
14. C. Louro, A. Cavaleiro, S. Dub, P. Smid, J. Musil, and J. Vlcek: The depth profile analysis of W–Si–N coatings after thermal annealing. *Surf. Coat. Technol.* **161,** 111 (2002).
15. H.J. Goldschmidt: *Interstitial Alloys* (Butterworth, London, U.K. 1967), p. 220.
16. M.G. Scott: Crystallization, in *Amorphous Metallic Alloys*, edited by F.E. Luborsky (Butterworths, London, U.K., 1983), Chap. 10.
17. J.G. Fleming, E. Roherty-Osmun, P.M. Smith, J.S. Custer, Y-D. Kim, T. Kacsich, M-A. Nicolet, and C.J. Galewski: Growth and properties of W–Si–N diffusion barriers deposited by chemical vapor deposition. *Thin Solid Films* **320,** 10 (1998).
18. J.P. Hirvonen, I. Suni, H. Kattelus, R. Lappalainen, P. Torri, H. Kung, T.R. Jervis, M. Nastasi, and J.R. Tesmer: Crystallization and oxidation behavior of Mo–Si–N coatings. *Surf. Coat. Technol.* **74–75,** 981 (1995).
19. H. Schmidt, W. Gruber, G. Borchardt, M. Bruns, M. Rudolphi, and H. Baumann: Thermal stability and crystallization kinetics of sputtered amorphous Si_3N_4 films. *Thin Solid Films* **450,** 346 (2004).
20. A. Niederhofer, P. Nesladek, H.D. Mannling, K. Moto, S. Veprek, and M. Jilek: Structural properties, internal stress and thermal stability of nc-TiN/a-Si_3N_4, nc-TiN/$TiSi_x$ and nc-$(Ti_{1-y}Al_ySi_x)N$ superhard nanocomposite coatings reaching the hardness of diamond. *Surf. Coat. Technol.* **120–121,** 173 (1999).
21. *Properties and Selection of Metals*, Metals Handbook, 8th ed. (ASM, Metals Park, OH, 1961, Vol. 1, pp. 502, 504, 511, and 817.
22. P.H. Townsend, D.M. Barnett, and T.A. Turner: Elastic relationships in layered composite media with approximation for the case of thin films on a thick substrate. *J. Appl. Phys.* **62,** 4438 (1987).
23. A. Ramalho, A. Cavaleiro, A.S. Miranda, and M.T. Vieira: Failure modes observed on worn surfaces of W–C–Co sputtered coatings. *Surf. Coat. Technol.* **62,** 536 (1993).
24. J.A. Thornton and W.D. Hoffman: Stress related effects in thin films. *Thin Solid Films* **171,** 5 (1989).
25. J.H. Moser, F. Tian, O. Haller, D.B. Bergstrom, I. Petrov, J.E. Greene, and C. Wiemer: Single-phase polycrystalline $Ti_{1-x}W_xN$ alloys ($0 \leqslant x \leqslant 0.7$) grown by UHV reactive magnetron sputtering: Microstructure and physical properties. *Thin Solid Films* **253,** 445 (1994).
26. M.F. Ashby: *Materials Selection in Mechanical Design* (Butterworth-Heinemann, London, U.K., 1992).
27. M.P. Hughey and R.F. Cook: Massive stress changes in plasma-enhanced chemical vapor deposited silicon nitride films on thermal cycling. *Thin Solid Films* **460,** 7 (2004).
28. Electronic Alloys U.K., http://www.aircraftmaterialsuk.com/data/electronic/al36.html.
29. L. Karlsson, A. Hörling, M.P. Johansson, L. Hultman, and G. Ramanath: The influence of thermal annealing on residual stresses and mechanical properties of arc-evaporated TiC_xN_{1-x} ($x = 0$, 0.15, and 0.45) thin films. *Acta Mater.* **50,** 5103 (2002).

30. Powder Diffraction File, Card No. 4-0806 (2000) (International Center for Diffraction Data, Philadelphia, PA).
31. J.V. Fernandes, A.C. Trindade, L.F. Menezes, and A. Cavaleiro: Influence of the substrate hardness on the W–C–Co coated samples to depth sensing indentation test. *J. Mater. Res.* **15,** 1766 (2000).
32. J. Musil, S. Kadlec, J. Vyskocil, and V. Valvoda: New results in dc reactive magnetron deposition of TiN_x films. *Thin Solid Films* **167,** 107 (1988).
33. H. Watanabe, Y. Sato, C. Nie, A. Ando, S. Ohtani, and N. Iwamoto: The mechanical properties and microstructure of Ti-Si-N nanocomposite films by ion plating. *Surf. Coat. Technol.* **169–170,** 452 (2003).
34. D. Ma, S. Ma, and K. Xu: Influence of Si content on nanostructured Ti-Si-N films coated by pulsed-dc plasma enhanced CVD. *Surf. Coat. Technol.* **184,** 182 (2004).
35. N. Jiang, Y.G. Shen, Y-W. Mai, T. Chan, and S.C. Tung: Nanocomposite Ti–Si–N films deposited by reactive unbalanced magnetron sputtering at room temperature. *Mater. Sci. Eng. B* **106,** 163 (2004).
36. J. Musil, F. Kunc, H. Zeman, and H. Polakova: Relationships between hardness, Young's modulus and elastic recovery in hard nanocomposite coatings. *Surf. Coat. Technol.* **154,** 304 (2002).
37. A. Matthews and A. Leyland: Developments in vapour deposited ceramic coatings for tribological applications. *Key Eng. Mater.* **206–213,** 459 (2002).